Biophysical *Journal*
Article

Biophysical Society

Kinetic Mechanisms of Fast Glutamate Sensing by Fluorescent Protein Probes

Catherine Coates,[1] Silke Kerruth,[1] Nordine Helassa,[1] and Katalin Török[1,*]
[1]Molecular and Clinical Sciences Research Institute, St. George's University of London, London, United Kingdom

ABSTRACT We have developed probes based on the bacterial periplasmic glutamate/aspartate binding protein with either an endogenously fluorescent protein or a synthetic fluorophore as the indicator of glutamate binding for studying the kinetic mechanism of glutamate binding. iGluSnFR variants termed iGlu$_h$, iGlu$_m$, and iGlu$_l$ cover a broad range of K_d-s (5.8 μM and 2.1 and 50 mM, respectively), and a novel fluorescently labeled indicator, Fl-GluBP, has a K_d of 9.7 μM. The fluorescence response kinetics of all the probes are consistent with a two-step mechanism involving ligand binding and isomerization either of the apo or the ligand-bound binding protein. Although the previously characterized ultrafast indicators iGlu$_u$ and iGlu$_f$ had monophasic fluorescence enhancement that occurred in the rate limiting isomerization step, the sensors described here all have biphasic binding kinetics with fluorescence increases occurring both in the glutamate binding and the isomerization steps. For iGlu$_m$ and iGlu$_l$, the data indicate prebinding conformational change followed by ligand binding. In contrast, for iGlu$_h$ and Fl-GluBP, glutamate binding is followed by isomerization. Thus, the effects of structural heterogeneity introduced by single amino acid changes around the binding site on the kinetic path of interactions with glutamate are revealed. Remarkably, glutamate binding with a diffusion-limited rate constant to iGlu$_h$ and Fl-GluBP is detected for the first time, hinting at the underlying mechanism of the supremely rapid activation of the highly homologous α-amino-3-hydroxy-5-methyl-4-isoxazolepropionic acid receptor by glutamate binding.

SIGNIFICANCE Protein-based fluorescent indicators are useful tools for investigating the mechanism of ligand-protein interactions both in vitro and in vivo. Here, we report the kinetic mechanisms of a number of glutamate indicator variants based on the bacterial periplasmic glutamate/aspartate binding protein, revealing the subtle differences in their kinetic pathway caused by the structural alteration of the glutamate binding protein by point mutations. Diffusion-limited glutamate binding indicated by a novel chemically labeled probe hints at the mechanism that underlies the rapid response of the α-amino-3-hydroxy-5-methyl-4-isoxazolepropionic acid receptor.

INTRODUCTION

Glutamate is a major excitatory neurotransmitter in the central nervous system; however, its synaptic and cellular dynamics have only become possible to investigate with high spatial and temporal resolution with the emergence of well-functioning optical sensors (1,2). The fastest fluorescent glutamate sensors iGluSnFR variants iGlu$_f$ and iGlu$_u$ have proved useful for tracking high frequency glutamate release at single hippocampal synapses (3) and revealed impaired glutamate clearance at striatal synapses in a Huntington's disease mouse model (4).

Information processing at synapses is rapid; glutamate neurotransmitter release is fast evoking α-amino-3-hydroxy-5-methyl-4-isoxazolepropionic acid receptor (AMPAR) channel opening with a time constant τ_{on} of 17 μs (5), making AMPAR the fastest responding ligand-gated ion channel. Glutamate clearance from the synapse is predicted to occur with τ_{off} of 50–200 μs (6,7). Visualizing synaptic and intracellular glutamate offers an important approach for better understanding of mechanisms of information processing at the synapse and of cellular glutamate homeostasis. For this, sensors with affinities and kinetics appropriate to the physiological conditions are required.

Submitted June 7, 2019, and accepted for publication November 11, 2019.

*Correspondence: ktorok@sgul.ac.uk

Catherine Coates's present address is The Institute of Cancer Research, Chester Beatty Laboratories, 237 Fulham Road, London, SW3 6JB, United Kingdom.

Silke Kerruth's present address is Faculty Education Office (Medicine), Imperial College London, South Kensington Campus, Sir Alexander Fleming Building, London SW7 2AZ, United Kingdom.

Nordine Helassa's present address is Department of Cellular and Molecular Physiology, Institute of Translational Medicine, University of Liverpool, Crown Street, Liverpool L69 3BX, United Kingdom.

Editor: Doug Barrick.

https://doi.org/10.1016/j.bpj.2019.11.006

Fluorescent glutamate sensors were initially developed from the extracellular domains of AMPAR, constructs of which are termed S1S2, and later from the bacterial periplasmic glutamate/aspartate binding protein (GluBP). GluR2-AMPAR-derived S1S2 constructs labeled with synthetic fluorophores were promising candidates for the generation of a glutamate biosensor but have proved impractical because of low refolding yield and stability (8). After extensive engineering, stable fluorescent S1S2 derivatives with high fluorescence dynamic ranges have been reported (9,10). For a fluorescent S1S2 derivative eEOS, an association rate constant of 1.2×10^5 $M^{-1}s^{-1}$ and an off rate of 14 s^{-1} were measured at 25°C (10), not representative of the rapid AMPAR glutamate interaction kinetics.

Bacterial periplasmic ligand binding proteins have been widely used for the generation of fluorescent biosensors, initially by covalent derivatization with synthetic fluorophores (e.g., for inorganic phosphate (11) and amino acid and sugar ligands (12,13)). Ligand binding kinetics of members of the bacterial periplasmic ligand binding protein family have been measured by monitoring Trp fluorescence, revealing association rate constants in the order of 10^7 $M^{-1}s^{-1}$ (14). The AMPAR S1S2 domain shares structural homology with GluBP, resulting in similar glutamate binding kinetic parameters measured by Trp fluorescence changes (15). The mechanism derived from these investigations was termed the Venus flytrap, whereby slow ligand binding is followed by a rapid conformational change, representing domain closure to trap the bound ligand. However, as Trp fluorescence served as an indicator of the conformational change, not of the binding, these experiments did not reveal the true association rate constant for glutamate.

In the genetically encoded glutamate sensor iGluSnFR, two separated fragments of GluBP were fused at each terminus of circularly permuted (cp) enhanced green fluorescent protein (EGFP). Fluorescence enhancement is based on two flanking portions of GluBP (large fragment GluBP 1–253, depicted as $iGlu_l$ and small fragment GluBP 254–279, depicted as $iGlu_s$) noncovalently reattaching on glutamate binding and thereby correcting the structure of cpEGFP. Apo-iGluSnFR has low fluorescence due to the low molar extinction coefficient at 492 nm (3); the highly fluorescent state, in which GluBP is reconstituted and stabilized by bound glutamate, is characterized by an increased ε_o(492 nm) and is represented as Glu.$iGlu_c$* (Fig. 1). Glu.$iGlu_c$* can be formed by one of two routes. In the first, the GluBP 1–253 ($iGlu_l$) fragment first binds glutamate; this is, however, not sufficient for fluorescence enhancement. Ligand binding is followed by a conformational change (the reattachment of GluBP 254–279 ($iGlu_s$) fragment to form the complete structure, depicted as $iGlu_c$), during which the highly fluorescent state develops. The rate of this isomerization step limits the fluorescence response (Fig. 1 and Scheme 1). Alternatively, if the separated fragments of GluBP have a higher affinity to reattach than to bind glutamate, binding would occur by conformational selection; a prebinding equilibrium would exist between $iGlu_l$-$iGlu_s$ and a reformed $iGlu_c$ with preferential ligand binding to $iGlu_c$ (Scheme 2 in Fig. 1). We have previously determined that the kinetic path that iGluSnFR, $iGlu_u$, and $iGlu_f$ follow corresponds to Scheme 1 (3).

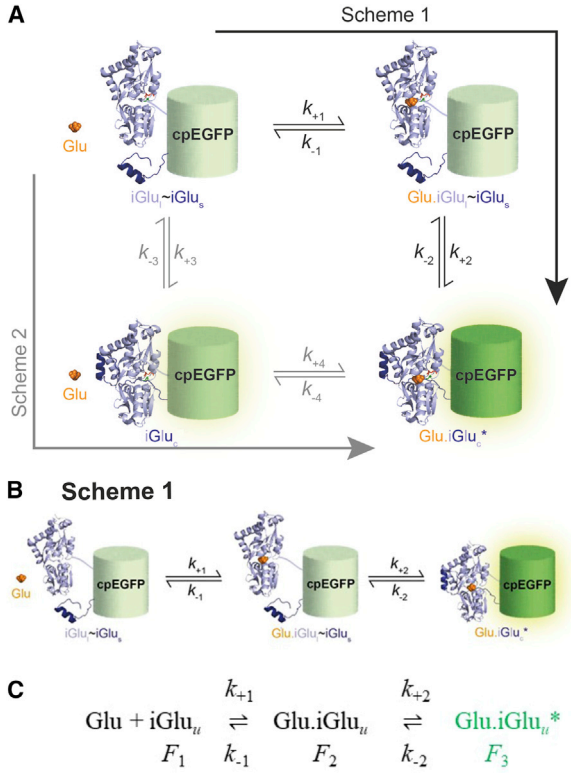

FIGURE 1 Alternative schemes for two-step protein-ligand interaction. (*A*) Shown are the kinetic paths of two-step mechanism involving ligand binding and isomerization applied to iGluSnFR and its fast variants $iGlu_u$ and $iGlu_f$ (mutated residues shown in green and red, respectively) (3). cpEGFP is flanked by a large fragment of GluBP residues 1–253 ($iGlu_l$) (*light blue ribbons*) and a small fragment of residues 254–279 ($iGlu_s$) (*dark blue ribbons*), which reattach on glutamate binding to form the highly fluorescent iGlu complete (Glu.$iGlu_c$*) with the corrected structure of cpEGFP. (*B*) Shown is a cartoon representation of Scheme 1 depicting the kinetic mechanism of iGluSnFR and fast variants $iGlu_u$ and $iGlu_f$ (3). (*C*) Scheme 1 is illustrated as a text equation using the example of ultrafast variant $iGlu_u$ (3). The structure of the bacterial periplasmic aspartate/glutamate binding protein (GluBP) (PDB: 2VHA) was adapted for the schematic illustration of an iGluSnFR variant.

To date, the fastest sensor $iGlu_u$ has τ_{on} of 460 μs in solution and τ_{off} of 2.7 ms (34°C) at Shaffer collaterals in hippocampal slices (3). That response time is concentration independent (3). We hypothesized that diffusion-limited glutamate binding occurs but is not indicated by the already characterized probes, and hence, we explore here the kinetic mechanism of a selection of affinity variants to see if they reveal rapid glutamate binding kinetics. Here, we demonstrate that the kinetic mechanisms of novel iGluSnFR

affinity variants (low affinity iGlu$_l$, medium affinity iGlu$_m$, and high affinity iGlu$_h$) are diverse. iGlu$_h$ follows Scheme 1, whereas iGlu$_l$ and iGlu$_m$ response occurs following the path depicted by Scheme 2. Furthermore, a novel sensor Fl-GluBP, generated by targeted Cys substitution of GluBP and derivatization with a synthetic fluorophore, displays diffusion-limited glutamate association kinetics. Such a mechanism is likely to underlie the AMPAR rapid response, and such a sensor has the potential for real-time glutamate tracking at single synapses under high frequency stimulation.

MATERIALS AND METHODS

Materials

pET41a iGlu$_m$ (R24K), pET41a iGlu$_h$ (E25A), pET41a iGlu$_l$ (T92A), and pET30b GluBP were generated as previously described (3) and are available on Addgene (Cambridge, MA) (119829, 119830, 119832, and 119835, respectively). *Escherichia coli* XL10-Gold and BL21(DE3) Gold cells were purchased from Stratagene (San Diego, CA). 6-Acryloyl-2-dimethylaminonaphthalene (Acrylodan), 7-diethylamino-3-(4′-maleimidylphenyl)-4-methylcoumarin (CPM), N-((2-(iodoacetoxy)ethyl)-N-methyl)-amino-7-nitrobenz-2-oxa-1,3-diazole (IANBD) ester, and Oregon Green 488 maleimide were purchased from Life Technologies (Carlsbad, CA), and 6-bromoacetyl-2-dimethylaminonaphthalene (BADAN) was purchased from Eurogentec (Liège, Belgium). N-(2-(iodoacetamido)ethyl)-7-diethylaminocoumarin-3-carboxamide (IDCC) was a gift from J.E.T. Corrie (National Institute for Medical Research, London, UK).

Site-directed mutagenesis

Ser or Thr to Cys mutations were introduced into pET30b GluBP via site-directed mutagenesis, according to the QuikChange II XL protocol (Agilent Technologies, Santa Clara, CA), using the following primers: T71C 5′-GCAGGTAAAACTGATTCCGATTTGCTCACAAAACCGTATTCC-3′, S72C 5′-TAAAACTGATTCCGATTACCTGCCAAAACCGTATTCCACT GCTG-3′, T83C 5′-CCACTGCTGCAAAACGGCTGTTTCGATTTTGAA TGTGGTTC-3′, S90C 5′-ACTTTCGATTTTGAATGTGGTTGTACCAC CAACAACGTC-3′, T91C 5′-CGATTTTGAATGTGGTTCTTGCACCAA CAACGTCGAACGC-3′, T92C 5′-GATTTTGAATGTGGTTCTACCTGC AACAACGTCGAACGCC-3′, T136C 5′-CAAAGCCGTAGTCGTCTGT TCCGGCACTACCTCTG-3′, S137C 5′-CGTAGTCGTCACTTGCGGCA CTACCTCTGAAG-3′, T140C 5′-GTCGTCACTTCCGGCACTTGCTCT GAAGTTTTGCTCAAC-3′, and A210C 5′-GCCGCAGTCTCAGGAG TGCTACGGTTGTATGTTG-3′.

DNA sequences were verified by sequencing (GENEWIZ UK, Bishop's Stortford, UK).

Protein expression and purification

iGluSnFR variants (iGlu$_l$, iGlu$_m$, and iGlu$_h$) and GluBP proteins (GluBP and GluBP-T136C) were expressed and purified as previously described (3). Briefly, cells were grown at 37°C until OD_{600nm} 0.5–1.0, and expression was induced with 0.4 mM isopropyl β-d-1-thiogalactopyranoside, overnight at 20°C. Cells were recovered by centrifugation and lysed by sonication on ice. Clarified lysates were purified by affinity purification (GSTrap or HisTrap; GE Healthcare, Little Chalfont, UK), and purity was assessed by sodium dodecyl sulfate polyacrylamide gel electrophoresis. Purified proteins were dialyzed overnight at 4°C in 50 mM HEPES-Na^+ and 200 mM NaCl (pH 7.5) and stored at −80°C.

Protein labeling with thiol-reactive environmentally sensitive fluorophores

Purified GluBP-T136C was labeled overnight at 4°C using a twofold excess of fluorophore (Acrylodan, IDCC, CPM, Oregon Green 488 Maleimide, BADAN, or IANBD). Labeled protein was then dialyzed three times over a 24-h period at 4°C against 500 volumes of phosphate-buffered saline to remove unreacted dye and then once against 300 volumes of assay buffer (50 mM HEPES-Na^+ (pH 7.5), 100 mM NaCl, and 2 mM $MgCl_2$) for buffer exchange.

Measurement of protein concentration

Protein concentration was determined by ultraviolet spectroscopy. For GluBP T136C-IANBD (Fl-GluBP), an extinction coefficient of 25,000 M^{-1} cm^{-1} at 495 nm was used, which corresponds to the absorbance peak of IANBD ester. For the His-GluBP protein and iGluSnFR variants (iGlu$_h$, iGlu$_m$, and iGlu$_l$), the extinction coefficients were 24,075 and 90,690 M^{-1} cm^{-1}, respectively, at 280 nm (16).

Dynamic range and affinity measurements

Measurements were carried out using a Fluorolog3 spectrofluorimeter (Horiba UK, Northampton, UK). For dynamic range determination, fluorescence emission spectra were recorded in the presence and absence of ligand. $F_{+ligand}/F_{-ligand}$ was calculated using values at the fluorescence emission maximum. For determination of ligand affinity and specificity (glutamate, aspartate, glutamine), ligand was added to the glutamate sensor (iGlu variant or labeled GluBP) either manually or via continuous titration (10 μL/min) using an automated syringe pump (Aladdin 1000; World Precision Instruments, Hitchin, UK). Measurements were performed in a stirred 3-mL cuvette containing protein in assay buffer. For iGluSnFR variants, $\lambda_{ex} = 492$ nm and $\lambda_{em} = 512$ nm, and for Fl-GluBP, $\lambda_{ex} = 495$ nm and $\lambda_{em} = 535$ nm was set. Data were corrected for dilution, normalized, and the dissociation constant (K_d) and Hill coefficient (n, when appropriate) were determined by fitting the data using the "one site specific binding" equation (with or without Hill slope as appropriate) in GraphPad Prism 7. Titrations were performed at least in triplicates, and the error was expressed as mean ± SD.

Stopped flow fluorimetry

Experiments were performed as detailed in (3) Helassa et al. Briefly, a KinetAsyst SF-61DX2 system (TgK Scientific, Bradford-on-Avon, UK) equipped with a temperature manifold (17) was used to measure kinetics. Fluorescence excitation was set to 492 nm, and fluorescence emission was collected using a long pass filter (>530 nm). For association kinetics, 0.25–0.7 μM protein (concentrations in the mixing chamber) was rapidly mixed with increasing concentrations of glutamate. For dissociation, GluBP was used in excess (915–1200 μM) and rapidly mixed with glutamate-bound sensor. The η values were calculated for 3°C using the density and viscosity calculator for glycerol/water mixtures based on Cheng (2008) at http://www.met.reading.ac.uk/~sws04cdw/viscosity_calc.html.

Data shown are the average of at least four traces; data were then fit using single or double exponentials (as appropriate) to ascertain the fluorescence rise or decay rate, using Kinetic Studio software (TgK Scientific). The error quoted is the standard error of the fit.

RESULTS

The domain structure of genetically encoded iGluSnFR affinity variants termed iGlu-T92A (iGlu$_l$), iGlu-R24K

($iGlu_m$), iGlu-E25A ($iGlu_h$), and chemically labeled Fl-GluBP are depicted in Fig. 2 *A*. Mutation sites for affinity variants and chemical labeling, respectively, were selected in the ligand binding site (Fig. 2 *B*). Equilibrium titrations with glutamate revealed a broad range of affinities with K_d-s from μM to tens of mM and fluorescence enhancements upon glutamate binding between 1.7 and 2.9-fold (Fig. 3 *A*; Table 1). The kinetic mechanisms of each of the four glutamate sensors will be presented, in turn revealing three different kinetic pathways.

Kinetic mechanism of high affinity sensor iGlu-E25A: $iGlu_h$

Of the genetically encoded variants, iGlu-E25A ($iGlu_h$) had the highest affinity for glutamate (K_d of 5.8 $\pm$ 0.2 μM) with $F_{(+Glu)}/F_{(-Glu)}$ of 3.4 $\pm$ 0.6 (Fig. 3 *A*; Table 1). Association kinetic experiments in which 0.5 μM $iGlu_h$ was rapidly mixed with glutamate at a series of concentrations showed a rapid rising phase of fluorescence followed by a second exponential fluorescence increase (Fig. 3 *B*).

The plot of the association rate of the second phase as a function of [Glu] had a hyperbolic appearance (Fig. 3 *C*). In that, $iGlu_h$ appears similar to iGluSnFR and fast variant $iGlu_f$ (3). However, the important distinction is that iGluSnFR and fast variant $iGlu_f$ had a low and a high fluorescence state, whereas $iGlu_h$ presents two enhanced fluorescence states, the first developing in the initial rapid process and the second in a measurable exponential process. iGluSnFR and fast variant $iGlu_f$ are represented by Scheme 1 above, in which binding without fluorescence increase is followed by isomerization in which fluorescence enhancement occurs. The mechanism for $iGlu_h$ is depicted in Scheme 1 (two fluorescent states), in which rapid binding of glutamate is also followed by a conformational change; however, both binding and isomerization induce separate fluorescence enhancements, the latter stabilizing the initially bound complex. For the initially bound complex to develop fluorescence enhancement, an intermediate with "semicomplete" (sc) structure $iGlu_{sc}$(E25A) is thus postulated, in which the separated GluBP fragments already have reattached. Glutamate binding to this gives Glu.$iGlu_{sc}$(E25A). A further structural rearrangement, possibly the closure of the cleft, then leads to the stable highly fluorescent complex Glu.$iGlu_c$(E25A)* (Scheme 1 (two fluorescent states)). Fluorescence enhancement in each phase is thought to be based on a shift of the equilibrium between the protonated, low-fluorescence form (with absorption maximum of 400 nm) and the deprotonated, high-fluorescence form that absorbs at 492 nm (18). Thus, increased brightness is expected to be based on the increase of the $\varepsilon_{o(492\ nm)}$ as found for iGluSnFR and fast variants $iGlu_u$ and $iGlu_f$ (3).

Dissociation kinetics were measured by trapping released glutamate from the complex of $iGlu_h$ with glutamate with >100-fold excess of purified GluBP (see Materials and

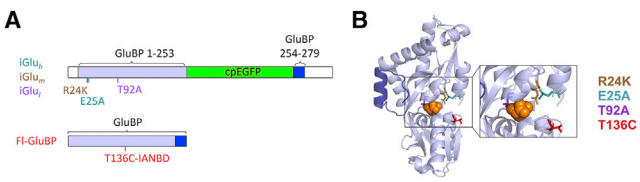

FIGURE 2 Design of iGluSnFR variants and Fl-GluBP. (*A*) Domain structure and labeling site is shown. (*B*) Shown is the crystal structure of GluBP (Protein Data Bank, PDB: 2VHA) with mutation sites indicated.

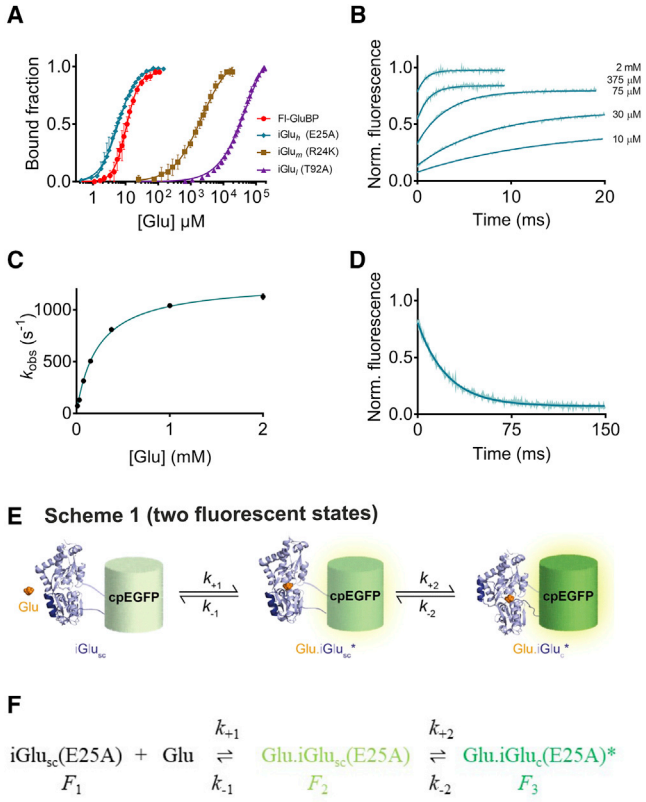

FIGURE 3 Equilibrium binding of novel sensors and kinetic mechanism of iGlu-E25A variant of iGluSnFR ($iGlu_h$). (*A*) Shown is the equilibrium titration with glutamate of iGlu variants and Fl-GluBP (20°C). Error bars represent SE. (*B*) Association kinetic records of iGlu-E25A ($iGlu_h$) (20°C) are shown. 0.25 μM $iGlu_h$ protein was rapidly mixed with different concentrations of glutamate. Solid lines are exponential fits to the data. (*C*) Shown is a plot of observed association rates (k_{obs}) against glutamate concentration for $iGlu_h$ fitted to Eq. 1. Error bars represent SD. (*D*) Shown are dissociation kinetics of $iGlu_h$ (20°C) fitted to a single exponential. (*E*) Shown is a cartoon representation and (*F*) illustration as a text equation of Scheme 1 (two fluorescent states) depicting the kinetic mechanism of $iGlu_h$. For the initially bound complex to develop fluorescence enhancement, an intermediate with "semicomplete" (sc) structure $iGlu_{sc}$(E25A) is postulated, in which the separated GluBP fragments have already reattached. Glutamate binding to this gives Glu.$iGlu_{sc}$(E25A). A further structural rearrangement, possibly the closure of the cleft, then leads to the stable highly fluorescent complex Glu.$iGlu_c$(E25A)* (Glu.$iGlu_c$*). The structure of the bacterial periplasmic aspartate/glutamate binding protein (GluBP) (PDB: 2VHA) was adapted for the schematic illustration of an iGluSnFR variant.

TABLE 1 Kinetic Parameters of iGlu$_l$, iGlu$_m$, iGlu$_h$, and FI-GluBP Obtained by Measurement

Temperature (°C)	Protein	K_d	n	k_{on}(lim) (s^{-1})	k_{off} (s^{-1})	τ_{off} (ms)	F_{+Glu}/F_{-Glu}
20	E25A (iGlu$_h$)	5.8 ± 0.2 μM	1.6 ± 0.1	1243 ± 32	42.2 ± 0.2	16.5	3.4 ± 0.6
20	T92A (iGlu$_l$)	50 ± 2 mM	1	1100 ± 1188	800[a]	1.25	1.7 ± 0.5
20	R24K (iGlu$_m$)	2.1 ± 0.1 mM	1	674 ± 503	365 ± 58	3.1	2.5 ± 0.4
20, 37	FI-GluBP (T136C)	9.7 ± 0.3 μM	2.2 ± 0.4	1128 ± 137	217 ± 5, 1997[b]	4.4, 0.5	2.9 ± 0.1
20, 34	iGlu$_u$[c]	600 μM	1.8	604, 3094[b]	468, 1481[b]	2.1, 0.7	3.8 ± 0.6
20, 34	iGlu$_f$[c]	137 μM	1.7	1227, 1493[b]	283, 478	3.5, 2.1	4.0 ± 0.3
20, 34	iGluSnFR[c]	33 μM	2.3	643, 799	110, 233	3.5, 2.1	5.4 ± 0.7

[a]Calculated value from model (Scheme 2) and on kinetics, with K_d as a constraint.
[b]Extrapolated from Arrhenius plots.
[c]Values, for illustration purposes, taken from (3).

Methods). Single exponential decay with a dissociation rate constant of 42.4 ± 0.2 s^{-1} (20°C) was measured (Fig. 3 *D*). Glutamate association kinetics would be described by $k_{obs1} = k_{+1}[Glu] + k_{-1}$ in pseudofirst order conditions; here, these were too fast to measure. Observed rates (k_{obs2}) obtained for the isomerization step were plotted as a function of [Glu]. A hyperbolic association rate plot was obtained, which was fitted to Eq. 1 (19). For detailed derivation of Eq. 1, also see Supporting Material in (3). The value for k_{-2} was fixed at the measured value of 42 s^{-1}. Best fit parameters were (3.92 ± 0.33) × 10^3 M^{-1} for K_1 and 1243 ± 32 s^{-1} for k_{+2}, indicating strong stabilization in the isomerization step. These parameters give a $K_{d(overall)}$ of 8.4 μM, which is within a twofold range of the 5.8 ± 0.2 μM measured by equilibrium titration, as follows:

$$k_{obs2} = k_{+2}K_1[Glu]/(1 + K_1[Glu]) + k_{-2}. \quad (1)$$

To estimate the order of magnitude of k_{+1}, the set of association kinetic records were subjected to global fitting, using k_{+2} 1243 s^{-1} and k_{-2} 42 s^{-1} to form the hyperbolic fit and with $K_{d(overall)}$ as a constraint. Global fitting indicated that values for $k_{+1} < 10^8$ $M^{-1}s^{-1}$ were insufficient to reproduce the rapid initial fluorescence increase. Using k_{+1} of 2.1 × 10^8 $M^{-1}s^{-1}$ and k_{-1} of 53,500 s^{-1} (corresponding to K_1 3.87 × 10^3 M^{-1}, a value close to 3.92 × 10^3 M^{-1} obtained from the fit to the hyperbole in Fig. 3 *C*), the fitted curves satisfactorily reproduced the data (see Supporting Materials and Methods). From the parameters of the global fit, the calculated $K_{d(overall)}$ was 8.4 μM. The high association rate constant indicated rapid, diffusion-limited glutamate binding to iGlu$_{sc}$(E25A). The strongly shifted equilibrium to Glu.iGlu$_c$(E25A)* is consistent with the observed single exponential dissociation kinetics.

Kinetic mechanism of low affinity sensor iGlu-T92A: iGlu$_l$

iGlu-T92A (iGlu$_l$) had the lowest affinity (K_d of 50 ± 2 mM) with glutamate-induced fluorescence enhancement $F_{(+Glu)}/F_{(-Glu)}$ of 1.7 ± 0.5 (Fig. 3 *A*; Table 1). The fluorescence enhancement of iGlu-T92A (iGlu$_l$), similarly to iGlu$_h$ above, also showed biphasic kinetics, a fast fluorescence increase with rates too fast to measure, followed by a single exponential fluorescence rise on glutamate binding with observed rates of up to 1200 s^{-1} (Fig. 4, *A* and *B*). However, the observed association rate, k_{obs2}, decreased as [glutamate] increased, plateauing at 400 s^{-1}. Such pattern of the association rate plot is consistent with a mechanism in which a slow pre-equilibrium exists between two forms of the apo protein, when glutamate binds to one of them preferentially (Scheme 2) (20). In the case of iGlu$_l$, two apo forms iGlu$_l$-iGlu$_s$(T92A) and iGlu$_c$(T92A), which has an elevated fluorescence intensity, are in equilibrium. Glutamate preferentially binds to iGlu$_c$(T92A), resulting in a further fluorescence enhancement.

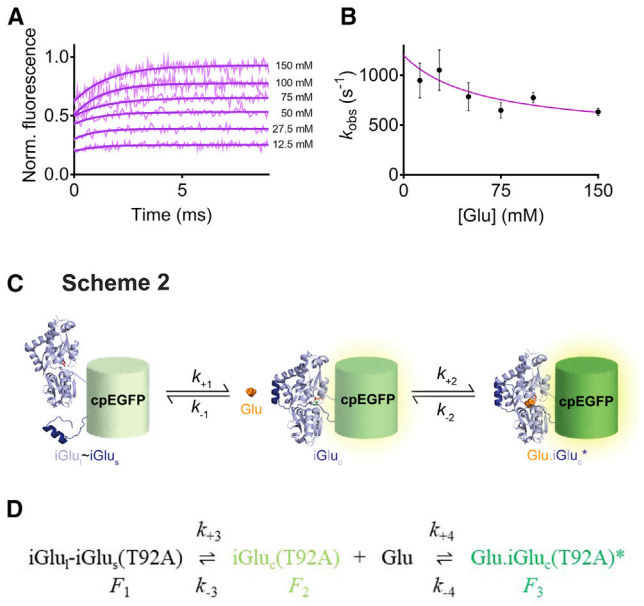

FIGURE 4 Kinetic mechanism of iGlu-T92A (iGlu$_l$). (*A*) Association kinetic records of iGlu-T92A (iGlu$_l$) (20°C) are shown. 0.7 μM iGlu$_l$ protein was rapidly mixed with different concentrations of glutamate. Solid lines represent exponential fits to the data. (*B*) Shown is a plot of observed association rates (k_{obs}) against glutamate concentration for iGlu$_l$. The solid line represents the fit to Eq. 3. Error bars represent SD. (*C*) Shown is a cartoon representation and (*D*) illustration as a text equation of Scheme 2 for iGlu$_l$. The structure of the bacterial periplasmic aspartate/glutamate binding protein (GluBP) (PDB: 2VHA) was adapted for the schematic illustration of an iGluSnFR variant.

The association rate plot in Fig. 4 *B* was fitted to Eq. 2, which represents the analytical solution for Scheme 2 (20). Best fit values to the data were k_{+3} of 361 ± 670 s^{-1}, k_{-3} of 739 ± 518 s^{-1}, and K_{d4} of 86 ± 212 mM (R^2 of 0.71), giving a $K_{d(overall)}$ of 28 mM (the measured value was 50 ± 2 mM). Using parameters close to the mean values (k_{+3} of 400 s^{-1} and k_{-3} of 800 s^{-1}) for global fitting of the association kinetic data, k_{+4} of 2 × 10^6 $M^{-1}s^{-1}$ and k_{-4} of 85,000 s^{-1} were obtained (see Supporting Materials and Methods). Dissociation kinetics were not possible to measure for $iGlu_l$, given the combination of its low affinity and fluorescence dynamic range:

$$k_{obs2} = k_{+3} + k_{-3}K_{d4}/(K_{d4} + [Glu]). \quad (2)$$

Kinetic mechanism of medium affinity sensor iGlu-R24K: $iGlu_m$

iGlu-R24K ($iGlu_m$) is a medium affinity probe (K_d of 2.1 ± 0.1 mM) with $F_{(+Glu)}/F_{(-Glu)}$ of 2.5 ± 0.4 (Fig. 3 *A*; Table 1). Like iGlu-T92A ($iGlu_l$), iGlu-R24K ($iGlu_m$) showed biphasic kinetics; a fast fluorescence increase with rates too fast to measure was followed by a single exponential fluorescence rise on glutamate binding with observed rates of up to 675 s^{-1} (Fig. 5, *A* and *B*). The observed association rate, k_{obs2}, decreased as [glutamate] was increased, plateauing at 350 s^{-1}. Such pattern of the association rate plot is consistent with a mechanism in which a slow pre-equilibrium exists between two forms of the apo protein, when glutamate binds to one of them preferentially (Scheme 2). When $iGlu_m$, $iGlu_l$-$iGlu_s$(R24K), and $iGlu_c$(R24K) are in equilibrium, glutamate binds to $iGlu_c$(R24K) preferentially. $iGlu_c$(R24K) has greater fluorescence intensity than $iGlu_l$-$iGlu_s$(R24K), and glutamate binding results in a further fluorescence enhancement. Dissociation kinetics were measured by trapping released glutamate from the complex of Glu_m with glutamate with >100-fold excess of purified GluBP (see Materials and Methods). A single exponential fluorescence decay was obtained for Glu_m with a rate of 365 ± 58 s^{-1} (20°C) (Fig. 5 *C*). The lack of an initial fast phase and the only partial fluorescence decrease in the dissociation record indicated that significant rebinding of glutamate occurred in the conditions used. The association rate plot data were fitted to Eq. 2 (20) and gave the following set of parameters for Glu_m: K_{d4}, 2.3 ± 13.1 mM; k_{+3}, 436 ± 146 s^{-1}; and k_{-3}, 238 ± 357 s^{-1} (R^2 0.72). The $K_{d(overall)}$ calculated from the fitted values is 1.5 mM, which is in good agreement with the measured value of 2.1 ± 0.1 mM. Global fit gave k_{+4}, 6 × 10^6 $M^{-1}s^{-1}$ and k_{-4}, 18,000 s^{-1}, resulting in K_4 of 3 mM and $K_{d(overall)}$ of 1.1 mM (see Supporting Materials and Methods).

As illustrated in Fig. 1, Scheme 1 and Scheme 2 represent two pathways, leading to the same final product. In the case of $iGlu_m$, the variation of association k_{obs} is relatively minor, and the trend can be taken as concentration independent.

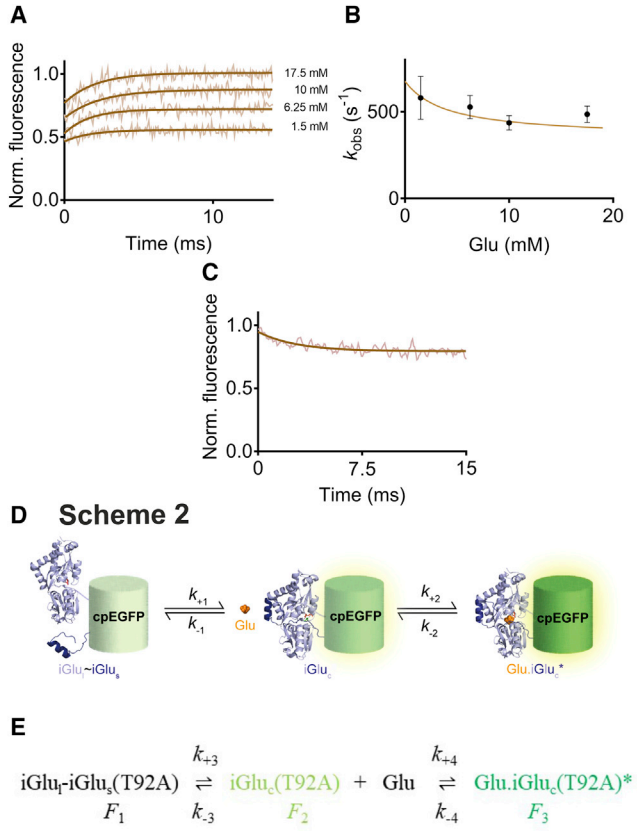

FIGURE 5 Kinetic mechanism of iGlu-R24K ($iGlu_m$). (*A*) Association kinetic records of iGlu-R24K ($iGlu_m$) (20°C) are shown. 0.5 μM $iGlu_m$ protein was rapidly mixed with different concentrations of glutamate. Solid lines represent exponential fits to the data. (*B*) Shown is a plot of observed association rates (k_{obs}) against glutamate concentration for $iGlu_m$. Error bars represent SD. (*C*) Dissociation kinetics of $iGlu_m$ (20°C) are shown. (*D*) Shown is a cartoon representation and (*E*) illustration as a text equation of Scheme 2 for $iGlu_m$. The structure of the bacterial periplasmic aspartate/glutamate binding protein (GluBP) (PDB: 2VHA) was adapted for the schematic illustration of an iGluSnFR variant.

The mean value of the observed rates k_{+2} + k_{-2} is 507 s^{-1}. Global fitting of the data to Scheme 1 (two fluorescent states) results in a similarly good fit with k_{+1} of 4 × 10^6 $M^{-1}s^{-1}$, k_{-1} of 16,000 s^{-1}, k_{+2} 135, and k_{-2} of 365 s^{-1}, giving $K_{d(overall)}$ of 2.9 mM. Thus, for $iGlu_m$, it is not possible to distinguish between the kinetic paths taken.

Development and kinetic mechanism of Fl-GluBP

GluBP variants T71C, S72C, T83C, S90C, T92C, T136C, S137C, T140C, and A210C were generated and covalently labeled with environmentally sensitive fluorophores acrylodan, BADAN, CPM, IDCC, IANBD ester, and Oregon Green 488 maleimide (Fig. 6). Fluorescently labeled derivatives were tested for fluorescence dynamic range, ligand selectivity, and kinetic response to ligand binding. Of all the combinations tested, IANBD-GluBP-T136C (termed Fl-GluBP) stood out with a 2.9-fold fluorescence enhancement upon

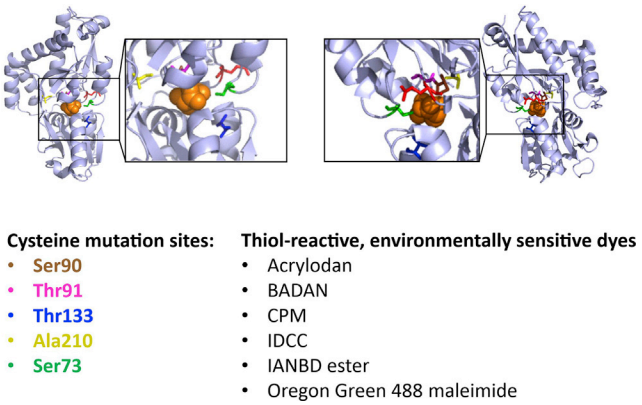

FIGURE 6 Mutation sites and fluorophores in the design of chemically labeled fluorescent glutamate sensor. The structure of the bacterial periplasmic aspartate/glutamate binding protein (GluBP) (PDB: 2VHA) was adapted to illustrate the mutation sites.

glutamate binding; none of the other combinations yielded greater than 10% fluorescence change. The K_d of Fl-GluBP for glutamate was 9.7 ± 0.3 μM (Fig. 3 A; Table 1) at physiological ionic strength, pH 7.5 and 20°C, ~20-fold increased from the 600 nM reported for GluBP (21).

The kinetics of the interaction of Fl-GluBP with glutamate were investigated by fluorescence stopped flow at 3°C (Fig. 7 *A*). Phenomenologically, a kinetically similar mechanism to that in Scheme 1 (two fluorescent states) was observed for a novel chemically labeled glutamate sensor, Fl-GluBP; however, the mechanism of fluorescence enhancement is different, based on polarity change around the synthetic fluorophore. The scheme depicting Fl-GluBP kinetic mechanism is thus termed Scheme 1 (synthetic).

For association kinetic experiments, as the glutamate concentration increased, it became apparent that the measured single exponential rise is preceded by a jump to a level that represents most of the fluorescence increase, indicating that at saturating concentrations, the first phase of the interaction—~90% of the fluorescence enhancement—was too fast to measure. Rates in the range of 200–800 s^{-1}, showing saturation, were measured for the second phase, interpreted as an isomerization. Plotting the isomerization rate (k_{obs}) as a function of glutamate concentration, a hyperbolic concentration dependence was observed (Fig. 7 *B*). Dissociation kinetics were obtained by rapidly mixing saturated 0.5 μM Fl-GluBP (33 μM glutamate) with 457 μM GluBP. A single exponential fluorescence decay at a rate of 217 ± 5 s^{-1} was observed at 3°C (Fig. 7 *C*), extrapolated to 1003 s^{-1} at 37°C based on a linear Arrhenius plot (Fig. 7 *C*, inset).

The kinetic data measured at 3°C for Fl-GluBP were interpreted in terms of a two-step mechanism in which rapid glutamate binding is followed by isomerization (Scheme 1 synthetic). Best fit parameters to the hyperbole in Fig. 7 *B* were as follows: K_1' of 6957 ± 131 M^{-1}, k'_{+2} of 1128 ± 137 s^{-1}, and k'_{-2} of 230 s^{-1} (fixed constant), giving

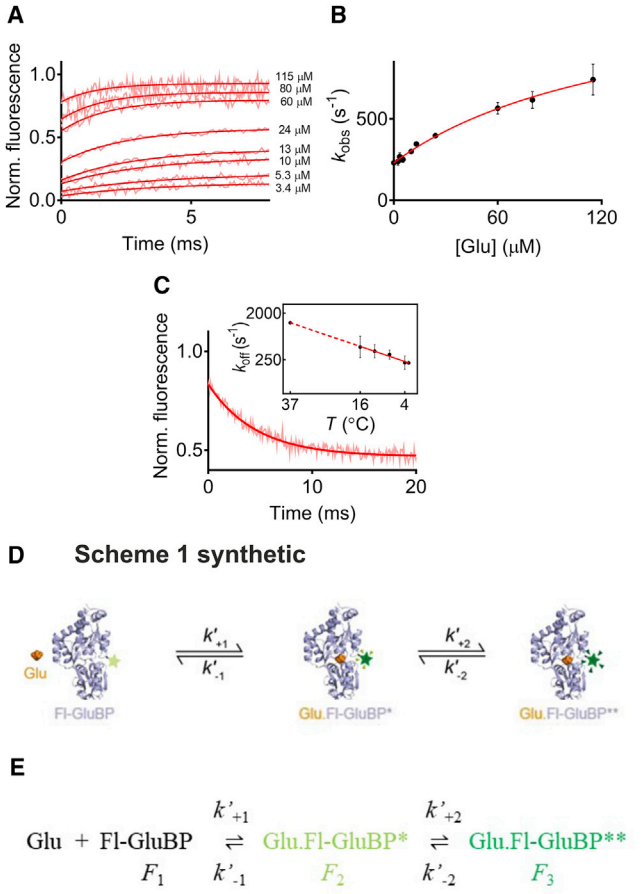

FIGURE 7 Kinetic mechanism of Fl-GluBP. (*A*) Association kinetic records of Fl-GluBP (3°C) are shown. 0.5 μM Fl-GluBP protein was rapidly mixed with different concentrations of glutamate. Solid lines are exponential fits to the data. (*B*) Shown is a plot of observed association rates (k_{obs}) against glutamate concentration for Fl-GluBP. (*C*) Dissociation kinetics of Fl-GluBP (3°C) are shown. Inset: Arrhenius plot of temperature dependence of the off rate is shown. Error bars represent SD. (*D*) Shown is a cartoon representation and (*E*) illustration as a text equation of Scheme 1 synthetic for Fl-GluBP. The structure of the bacterial periplasmic aspartate/glutamate binding protein (GluBP) (PDB: 2VHA) was adapted for the schematic illustration of an iGluSnFR variant.

$K_{d(overall)}$ 24 μM, comparable to the measured 9.7 ± 0.3 μM (Fig. 3 *A*; Table 1). To obtain a good global fit to the association kinetic record, a k'_{+1} of greater or equal to 10^9 $M^{-1}s^{-1}$ was required, indicating diffusion-limited glutamate binding. Further parameter values obtained from the global fit were as follows: k'_{-1} of 216,000 s^{-1}, k'_{+2} of 2220 s^{-1} and k'_{-2} of 230 s^{-1} ($K_{d(overall)}$ 20.2 μM).

Kinetics of glutamate binding to Fl-GluBP under increased viscosity

We measured the association kinetics of Fl-GluBP at increasing solvent viscosities to see if the diffusion-limited glutamate binding step is affected. Relative viscosity (η) was increased up to sixfold. Interestingly, the amplitude of

fluorescence enhancement, rather than the rate of binding, was affected. Holding [glutamate] at 50 μM (in the mixing chamber), the rapid binding step appeared as a progressively smaller "jump" in fluorescence intensity and was completely abolished in 60% glycerol (Fig. 8 *A*). The disappearance of the initial fast fluorescence was the result of the apo state fluorescence intensity increasing with greater viscosity. Increasing solvent viscosity thus had a similar effect on the fluorescence intensity of apo-Fl-GluBP to glutamate binding. At relative viscosity η of 6, the glutamate binding invoked fluorescence increase purely reflected the conformational change of the protein.

In contrast, the rate of isomerization was slowed down from 600 to 400 s^{-1} at 50–60% glycerol (Fig. 8 *B*). Applying a previously developed theory (22) from the foundation laid down in (23) for the effect of solvent viscosity on first order processes, we obtained a good fit for our isomerization data to Eq. 3, where C and σ (σ has units of viscosity) are adjustable parameters, and η is solvent viscosity. The pattern of the rate plot fits well to the theory that in the viscosity range examined, both internal friction of the protein and friction of the molecule with the solvent contribute to decreasing the rate constant (22) (Fig. 8 *B*). The fitted values gave C = 1.96 × 10^8 cP/s^{-1}, σ = 40.45 cP, and E_o = 4.87 kcal/mol^{-1}. The small activation energy indicates that most of the change in the rate constant is due to the change in viscosity (22):

$$k_{obs} = C * exp(-E_o / RT)/(s+h). \quad (3)$$

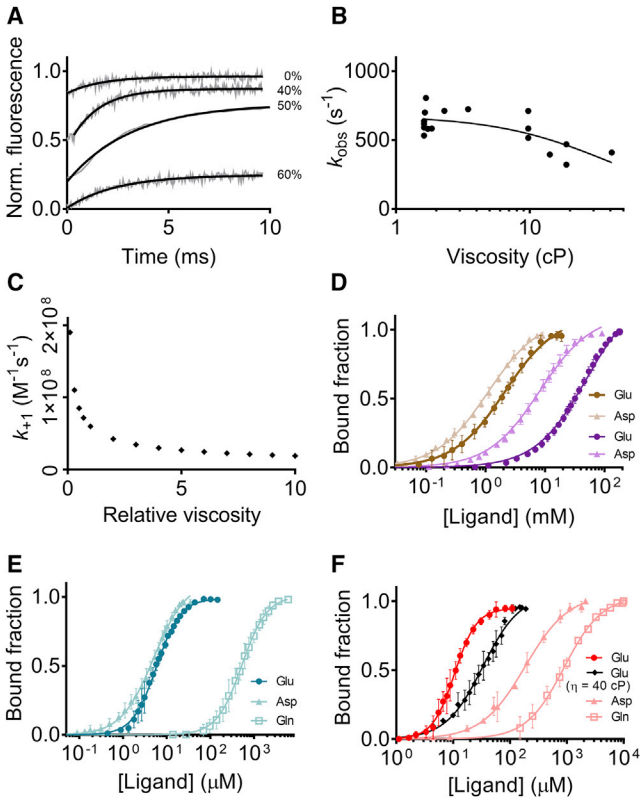

FIGURE 8 Viscosity dependence and selectivity. (*A*) Shown are association kinetic records for Fl-GluBP in solvents with increasing viscosity at 3°C. (*B*) Shown is a plot of observed rates (k_{obs}) against relative viscosity for Fl-GluBP. Measured values were fitted to Eq. 3 (*solid line*). (*C*) Shown is a plot of predicted second order rate constant as a function of relative viscosity at 3°C. (*D*) Shown is equilibrium titration of iGlu-T92A (iGlu$_l$) (*purple symbols* and *lines*) and iGlu-R24K (iGlu$_m$) (*terracotta symbols* and *lines*) with glutamate and aspartate at 20°C. Error bars represent SE. (*E*) Shown is equilibrium titration of iGlu-E25A (iGlu$_h$) with glutamate, aspartate, and glutamine at 20°C. Error bars represent SE. (*F*) Shown is equilibrium titration of Fl-GluBP with glutamate (in 0 and 60% glycerol) at 3°C and aspartate and glutamine at 20°C. Error bars represent SE.

Ligand selectivity of iGlu$_l$, iGlu$_m$, iGlu$_h$, and Fl-GluBP

Each of the mutations giving iGlu$_l$, iGlu$_m$, and iGlu$_h$ shifted the selectivity toward aspartate, which does not disqualify these variants from investigations at excitatory synapses in the hippocampus, in which glutamate fully accounts for neurotransmission (24). The selectivity for glutamate over glutamine is a more complex issue. The lowest affinity variants iGlu$_l$ and iGlu$_m$ appear to show the highest selectivity for glutamate, whereas their response to glutamine is hardly detectable. Fl-GluBP is highly selective for glutamate (K_d 10.6 ± 2.3 μM) over aspartate (K_d 184 ± 15 μM) and glutamine (K_d 896 ± 55 μM) as well as having smaller 1.7- and 2.5-fold fluorescence enhancements, respectively (Fig. 8 *F*; Table 2). However, in an environment where both glutamate and glutamine are present, iGlu$_h$ and Fl-GluBP could yield composite signals due to their affinities being relevant to the physiological concentration ranges and high fluorescence dynamic range for both ligands (Fig. 8, *D* and *E*; Table 2). At 100 μM glutamate, for example, Fl-GluBP would be saturated while giving only 10% of the signal at 100 μM glutamine. However, Fl-GluBP would function well in the synaptic cleft where glutamine concentration is negligible. In turn, Fl-GluBP may also be suitable for detecting glutamine in an environment in which glutamate concentration is negligible. D-Ser, glycine, and γ-aminobutyric acid do not evoke any fluorescence response from Fl-GluBP (data not shown).

DISCUSSION

Protein-based fluorescent glutamate sensors have the potential for real-time monitoring of synaptic and cellular glutamate concentration changes. We have developed both genetically encoded and chemically labeled fluorescent glutamate sensors and characterized the kinetic mechanisms of their glutamate sensing. Previously described iGlu$_f$ and iGlu$_u$ responded to glutamate binding with a single exponential fluorescence increase, which occurred in an isomerization step after glutamate binding (Scheme 1) (3). Novel variants, iGlu$_l$ and iGlu$_m$, with mM affinity for glutamate,

TABLE 2 Kinetic Parameters of iGlu$_l$, iGlu$_m$, iGlu$_h$, and Fl-GluBP Fitted to Their Respective Mechanisms

	Temperature (°C)	Protein	K_d (μM)	K_4 (M^{-1})	k_{+4} ($M^{-1}s^{-1}$)	k_{-4} (s^{-1})	k_{+3} (s^{-1})	k_{-3} (s^{-1})	F_1	F_2	F_3
Scheme 2	20	T92A (iGlu$_l$)	28,000	12	2×10^6	85,000	400	800	0.86	1.3	1.7
Scheme 2	20	R24K (iGlu$_m$)	1060	333	6×10^6	18,000	436	238	0.68	1.3	2.5
	Temperature°C	Protein	K_d (μM)	K_1 (M^{-1})	k_{+1} ($M^{-1}s^{-1}$)	k_{-1} (s^{-1})	k_{+2} (s^{-1})	k_{-2} (s^{-1})	F_1	F_2	F_3
Scheme 1 (two fluorescent states)	20	E25A (iGlu$_h$)	8.4	3870	2.1×10^8	53,500	1243	42	1	3.2	3.4
Scheme 1 synthetic	3	Fl-GluBP (T136C)	20	6957	10^9	216,000	1128	230	1	2.7	2.9
Scheme 1	20	iGlu$_u$	600	1291	2.2×10^6	1704	136	468	1	1	13.4
Scheme 1	20	iGlu$_f$	147	1587	3.5×10^6	2206	944	283	1	1	4.9
Scheme 1	20	iGluSnFR	44	5184	2.7×10^7	5965	533	110	1	1	6.3

K_d represents calculated $K_{d(overall)}$ from data fitted to Eq.1, giving K_1, k_{+2}, and k_{-2}, or Eq. 2, giving K_4, k_{+3}, and k_{-3}, as appropriate. These parameters were fed into global fitting to obtain k_{+1} and k_{-1} and k_{+4} and k_{-4}, respectively. Underlined are the relative fluorescence values of the species, between which is the glutamate binding step. Isomerization occurs either of the apo or the glutamate-bound form. For Scheme 1-type reactions, relative fluorescence values are related by the equation $F\infty = (k_{+2}\,F_3 + k_{-2}\,F_2)/(k_{+2} + k_{-2})$ (30). F_1 is defined for the apo state as 1, and $F_\infty = F_{+Glu}/F_1$ (see F_{+Glu}/F_{-Glu} in Table 1). F_2 is the proportion of fluorescence enhancement in the fast phase taken at saturating concentrations. As for both iGlu$_h$ and Fl-GluBP, $k_{+2} >> k_{-2}$, $F_3 \sim F_\infty$. For Scheme 2, F_1 is calculated from the isomerization equilibrium in which $1 = (k_{+3}\,F_2 + k_{-3}\,F_1)/(k_{+3} + k_{-3})$. Here, $F_3 = F_\infty$ at saturating concentrations.

follow an alternative kinetic path, whereby reattachment of GluBP fragments, accounting for part of the fluorescence enhancement, is required for glutamate to bind to the reformed complex, which causes further fluorescence enhancement (Scheme 2). For iGlu$_l$ and iGlu$_m$, the conformer with the separate large and small GluBP fragments is in an equilibrium with the reassembled, "complete" GluBP (a low-fluorescence conformer), to which glutamate preferentially binds, followed by most of the fluorescence enhancement. It is likely that the binding is followed by an open-to-closed transition, and the two are seen in combination in the rapid fluorescence rise. It must be noted that with the exception of iGlu$_l$ and iGlu$_m$, equilibrium titration curves are best fit to the Hill equation, giving Hill coefficient (n) values of 1.6–2.3. However, as the kinetic analyses reveal, none of the kinetic data indicate cooperativity of binding. Therefore, $n = 1$ is used in the kinetic analyses.

Glutamate binding to iGlu$_h$ is followed by isomerization (Scheme 1 (two fluorescent states)). Fluorescence enhancement of iGlu$_h$ is biphasic, with most of the increase occurring in the diffusion-limited glutamate binding phase, indicating that apo-GluBP in this variant exists in a sc conformation in which the small fragment may already be attached to the large fragment, albeit not in a stable conformation. iGlu$_m$ isomerization showed a shallow concentration dependence in the association kinetics. These data are compatible with either Scheme 2 or Scheme 1 (two fluorescent states).

Fl-GluBP, a glutamate sensor generated by fluorescent derivatization of GluBP with a synthetic fluorophore, also yields most of its fluorescence enhancement in the initial glutamate binding phase, which occurs with a diffusion-limited rate constant (Scheme 1 synthetic). A subsequent isomerization further stabilizes the fluorescent complex. The rate of isomerization for Fl-GluBP is fitted to saturate at 2220 s^{-1} at 3°C, indicating that Fl-GluBP will be suitable as a real-time tracker of synaptic glutamate transients.

Although we were therefore unable to measure the second order rate constant (k_{+1}) for glutamate binding, even at increased solvent viscosity, we attempt to estimate it. An inverse relationship between rate constant and viscosity has been reported (25). Reasoning that for it to be too fast to measure at 3°C and have a relative viscosity of 6 at 50 μM glutamate, the observed association rate needs to be >1000 s^{-1}, $k_{+1} > 2 \times 10^7$ $M^{-1}s^{-1}$ is required. At relative viscosity of 1, k_{+1} is predicted to be 10-fold higher, $>2 \times 10^8$ $M^{-1}s^{-1}$ at 3°C (Fig. 8 *C*). Assuming a twofold increase for every 5°C increase in temperature, $k_{+1} > 2 \times 10^9$ $M^{-1}s^{-1}$ at 20°C and $k_{+1} > 3 \times 10^{10}$ $M^{-1}s^{-1}$ 37°C are predicted. If another empirical formula in which there is an inverse relationship between diffusion-controlled reaction rate constant and the square root of relative viscosity is used (26), the estimates are in the same range. These values are consistent with diffusion-limited glutamate association

TABLE 3 Affinity and Selectivity of Fl-GluBP, iGlu$_h$, iGlu$_m$, and iGlu$_l$ for L-Aspartate and L-Glutamine

Protein	$F_{(+Glu)}/F_{(-Glu}$	$K_{d(Glu)}$	n	$F_{(+Asp)}/F_{(-Asp)}$	$K_{d(Asp)}$	n	$F_{(+Gln)}/F_{(-Gln)}$	$K_{d(Gln)}$	n
iGlu$_l$ (T92A)	1.7 ± 0.5	50 ± 2 mM	1	2.5 ± 0.1	8.2 ± 0.3 mM	1	1.1 ± 0.1	N.A.	N.A.
iGlu$_m$ (R24K)	2.5 ± 0.4	2.1 ± 0.1 mM	1	1.8 ± 0.1	1.1 ± 0.1 mM	1	1.1 ± 0.1	≥ 38 mM	1
iGlu$_h$ (E25A)	3.4 ± 0.6	5.8 ± 0.2 μM	1.6 ± 0.1	4.5 ± 0.1	5.0 ± 0.4 μM	1.2 ± 0.1	5.1 ± 0.4	523 ± 28 μM	1.5 ± 0.1
Fl-GluBP (T136C)	2.9 ± 0.1	10.6 ± 0.4 μM	2.3 ± 0.2	1.7 ± 0.1	184 ± 15 μM	1.1 ± 0.1	2.5 ± 0.1	896 ± 55 μM	1.3 ± 0.1
Fl-GluBP (T136C) $\eta = 6$	1.4 ± 0.1	33 ± 4 μM	1.3 ± 0.2	N.D.	N.D.	N.D.	N.D.	N.D.	N.D.

All measurements were carried out at 20°C with the exception of Fl-GluBP measurements, which were done at 3°C. N.A., not applicable as no change is detectable; N.D., not determined.

kinetics, which makes Fl-GluBP and $iGlu_h$ potential real-time detectors of synaptic glutamate release kinetics.

There is strong structural homology between GluBP and the S1S2 glutamate binding domain of AMPAR (Fig. 9). Neither iGluSnFR-type probes nor the previously studied Trp fluorescence changes allowed the observation of glutamate binding itself. The observed conformational changes by Trp fluorescence led to the Venus flytrap model for ligand binding to bacterial periplasmic binding proteins (14,27) and the homologous S1S2 glutamate binding construct derived from AMPAR (15), which does not explain the rapid opening of the AMPAR ion channel triggered by ligand glutamate binding. Neither can the $iGlu_u$ fluorescence response, which is based on a protein conformational change (3). The kinetic examination of Fl-GluBP and $iGlu_h$, however, reveals that they signal diffusion-limited binding of glutamate. We propose that a similar mechanism of diffusion-limited glutamate binding exists for and forms the basis of rapid gating of AMPAR.

Moreover, a fluorescent sensor like Fl-GluBP may be useful for measuring synaptic viscosity. This may be through the relative fluorescence measurements of the binding and isomerization steps or by lifetime imaging as the lifetime is expected to increase if a singlet-exciplex intermediate is formed (28,29).

The two low affinity glutamate sensors $iGlu_l$ and $iGlu_m$ have fast off rates of 800 s^{-1} (fitted value) and 365 s^{-1} (measured at 20°C), respectively. The off rate for Fl-GluBP is measured as 217 s^{-1} at 3°C and the extrapolated value at 37°C is 2000 s^{-1} from its Arrhenius plot. All three sensors would thus allow monitoring processes on the submillisecond timescale at the temperatures of physiological experiments (34–37°C). Through their broad affinity range and mechanistic variety, the above genetically encoded and chemically labeled fluorescent glutamate sensors could form part of a tool kit designed for monitoring the different processes that glutamate undergoes in neurotransmission and cellular homeostasis. Each variant would be best suited to indicate glutamate concentration changes in the range of their affinity.

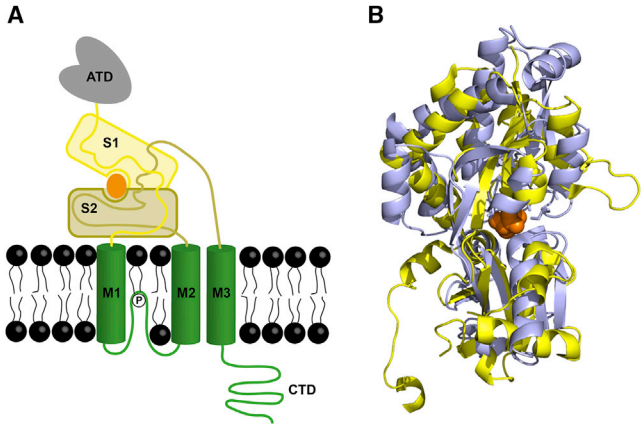

FIGURE 9 Structural alignment of AMPAR S1S2 glutamate binding domain (PDB: 5L1B) and bacterial glutamate/aspartate binding protein (PDB: 2VHA). (*A*) Shown is a schematic structure of AMPAR, illustrating the glutamate binding domain (S1S2). (*B*) The structures of GluBP and AMPAR S1S2 are aligned using Pymol software to reveal a high degree of structural homology.

The stopped flow association kinetic data reveal how each sensor would respond when glutamate is elevated. For example, the response rate of Fl-GluBP response near-proportionately increases with [Glu] in the tens of μM range. $iGlu_h$, up to ~0.2 mM [Glu], gives slow, concentration-dependent fluorescence responses, the rate and amplitude of which increases proportionately with [Glu] rate and is limited by the ligand binding rate. Above ~1 mM, the isomerization is rate limiting; thus, the response is concentration independent, saturating the probe. With $iGlu_l$, there is relatively little concentration dependence of the on kinetics, but the response amplitude increases through the tens of mM range.

Relative fluorescence and molecular brightness values for the intermediates were derived from the fold increase on glutamate binding, taking into account the isomerization equilibrium and estimation of F_2 from the association kinetic records to calculate F_3. These values, together with the full set of rate constants, allow simulation of the response (see Supporting Materials and Methods). Moreover, applying the observed rates at a particular glutamate concentration would allow calculation of the ratio of the amplitudes, from which the concentration of intermediates can be deduced (30).

In summary, this work reveals previously unseen kinetic properties and the kinetic mechanisms of fluorescent glutamate probes based on the bacterial periplasmic glutamate/aspartate binding protein. This family of ligand binding proteins has previously been described by the Venus flytrap mechanism in which slow binding is followed by rapid closure of the binding cleft. This was based on observing the fluorescence response of Trp residues, which evidently only reported the conformational change after binding. Here, we discovered that GluBP and a high affinity variant bind glutamate with a diffusion-limited rate constant. We further postulate that given the strong structural homology with the AMPAR binding domain, initial glutamate binding is limited by diffusion. Thus collision is sufficient to trigger the rapid change in the environment of the fluorophore, which is the binding site for channel opening of the AMPAR. Channel opening occurs within tens of microseconds not requiring the subsequent conformational change (likely domain closure). Our data furthermore highlight the kinetic diversity that arises from single residue mutations around the binding pocket.

CONCLUSION

Subtle structural changes brought about by single amino acid substitutions, in addition to affecting their ligand

binding affinity and selectivity, also redirect the kinetic paths of the fluorescence response of iGluSnFR variants. A novel probe labeled with a synthetic fluorophore reveals diffusion-limited glutamate binding, hints at the AMPAR response mechanism, and may be suitable for measuring synaptic viscosity.

SUPPORTING MATERIAL

Supporting Material can be found online at https://doi.org/10.1016/j.bpj.2019.11.006.

AUTHOR CONTRIBUTIONS

C.C. and S.K. generated the genetically encoded proteins, performed experiments, analyzed data, and generated figures. N.H. generated the chemically labeled probes. K.T. designed the project and wrote the article.

ACKNOWLEDGMENTS

Dr. Alamin Mohammed is thanked for comments on the manuscript. Melissa Matthews is thanked for her help with the characterization of the R24K iGluSnFR variant.

This work was funded by Wellcome Trust grant 094385/Z/10/Z and Biotechnology and Biological Sciences Research Council grants BB/M02556X/1 and BB/S003894/1 to K.T.

REFERENCES

1. Marvin, J. S., B. G. Borghuis, …, L. L. Looger. 2013. An optimized fluorescent probe for visualizing glutamate neurotransmission. *Nat. Methods.* 10:162–170.
2. Marvin, J. S., B. Scholl, …, L. L. Looger. 2018. Stability, affinity, and chromatic variants of the glutamate sensor iGluSnFR. *Nat. Methods.* 15:936–939.
3. Helassa, N., C. D. Dürst, …, K. Török. 2018. Ultrafast glutamate sensors resolve high-frequency release at Schaffer collateral synapses. *Proc. Natl. Acad. Sci. USA.* 115:5594–5599.
4. Dvorzhak, A., N. Helassa, K. Török, D. Schmitz, and R. Grantyn. 2019. Single synapse indicators of impaired glutamate clearance derived from fast $iGlu_u$ imaging of cortical afferents in the striatum of normal and Huntington (Q175) mice. *J. Neurosci.* 39:3970–3982.
5. Li, G., W. Pei, and L. Niu. 2003. Channel-opening kinetics of GluR2Q(flip) AMPA receptor: a laser-pulse photolysis study. *Biochemistry.* 42:12358–12366.
6. Scimemi, A., and M. Beato. 2009. Determining the neurotransmitter concentration profile at active synapses. *Mol. Neurobiol.* 40:289–306.
7. Zheng, K., T. P. Jensen, …, D. A. Rusakov. 2017. Nanoscale diffusion in the synaptic cleft and beyond measured with time-resolved fluorescence anisotropy imaging. *Sci. Rep.* 7:42022.
8. Best, S. L., J. E. T. Corrie, and K. Török. 2005. Development of a fluorescent glutamate binding protein. *Biophys. J.* 88:46a–47a.
9. Namiki, S., H. Sakamoto, …, K. Hirose. 2007. Optical glutamate sensor for spatiotemporal analysis of synaptic transmission. *Eur. J. Neurosci.* 25:2249–2259.
10. Takikawa, K., D. Asanuma, …, K. Hirose. 2014. High-throughput development of a hybrid-type fluorescent glutamate sensor for analysis of synaptic transmission. *Angew. Chem. Int.Engl.* 53:13439–13443.
11. Solscheid, C., S. Kunzelmann, …, M. R. Webb. 2015. Development of a reagentless biosensor for inorganic phosphate, applicable over a wide concentration range. *Biochemistry.* 54:5054–5062.
12. de Lorimier, R. M., J. J. Smith, …, H. W. Hellinga. 2002. Construction of a fluorescent biosensor family. *Protein Sci.* 11:2655–2675.
13. Kunzelmann, S., C. Solscheid, and M. R. Webb. 2014. Fluorescent biosensors: design and application to motor proteins. *Exp Suppl.* 105:25–47.
14. Miller, D. M., III, J. S. Olson, …, F. A. Quiocho. 1983. Rates of ligand binding to periplasmic proteins involved in bacterial transport and chemotaxis. *J. Biol. Chem.* 258:13665–13672.
15. Abele, R., K. Keinanen, and D. R. Madden. 2000. Agonist-induced isomerization in a glutamate receptor ligand-binding domain. A kinetic and mutagenetic analysis. *J. Biol. Chem.* 275:21355–21363.
16. Gill, S. C., and P. H. von Hippel. 1989. Calculation of protein extinction coefficients from amino acid sequence data. *Anal. Biochem.* 182:319–326.
17. Walklate, J., and M. A. Geeves. 2015. Temperature manifold for a stopped-flow machine to allow measurements from -10 to +40°C. *Anal. Biochem.* 476:11–16.
18. Barnett, L. M., T. E. Hughes, and M. Drobizhev. 2017. Deciphering the molecular mechanism responsible for GCaMP6m's Ca^{2+}-dependent change in fluorescence. *PLoS One.* 12:e0170934.
19. Bagshaw, C. R., J. F. Eccleston, …, D. R. Trentham. 1974. The magnesium ion-dependent adenosine triphosphatase of myosin. Two-step processes of adenosine triphosphate association and adenosine diphosphate dissociation. *Biochem. J.* 141:351–364.
20. Halford, S. E. 1971. *Escherichia coli* alkaline phosphatase. An analysis of transient kinetics. *Biochem. J.* 125:319–327.
21. Okumoto, S., L. L. Looger, …, W. B. Frommer. 2005. Detection of glutamate release from neurons by genetically encoded surface-displayed FRET nanosensors. *Proc. Natl. Acad. Sci. USA.* 102:8740–8745.
22. Ansari, A., C. M. Jones, …, W. A. Eaton. 1992. The role of solvent viscosity in the dynamics of protein conformational changes. *Science.* 256:1796–1798.
23. Kramers, H. A. 1940. Brownian motion in a field of force. *Physica (Utrecht).* 7:284–304.
24. Herring, B. E., K. Silm, …, R. A. Nicoll. 2015. Is aspartate an excitatory neurotransmitter? *J. Neurosci.* 35:10168–10171.
25. Masson, P., S. Lushchekina, …, O. Lockridge. 2013. Effects of viscosity and osmotic stress on the reaction of human butyrylcholinesterase with cresyl saligenin phosphate, a toxicant related to aerotoxic syndrome: kinetic and molecular dynamics studies. *Biochem. J.* 454:387–399.
26. Hasinoff, B. B., and S. B. Chishti. 1982. Viscosity dependence of the kinetics of the diffusion-controlled reaction of carbon monoxide and myoglobin. *Biochemistry.* 21:4275–4278.
27. Wolf, A., E. W. Shaw, …, G. F. Ames. 1995. Structure/function analysis of the periplasmic histidine-binding protein. Mutations decreasing ligand binding alter the properties of the conformational change and of the closed form. *J. Biol. Chem.* 270:16097–16106.
28. Berezin, M. Y., and S. Achilefu. 2010. Fluorescence lifetime measurements and biological imaging. *Chem. Rev.* 110:2641–2684.
29. Lajevardipour, A., J. W. Chon, …, A. H. Clayton. 2016. Imaging cellular dynamics with spectral relaxation imaging microscopy: distinct spectral dynamics in golgi membranes of living cells. *Sci. Rep.* 6:37038.
30. Török, K., and D. R. Trentham. 1994. Mechanism of 2-chloro-(epsilon-amino-Lys75)-[6-[4-(*N,N*- diethylamino)phenyl]-1,3,5-triazin-4-yl]calmodulin interactions with smooth muscle myosin light chain kinase and derived peptides. *Biochemistry.* 33:12807–12820.